

Numerical modelling and experimental validation of debonding and heat transfer of carbon fiber reinforced composite under reciprocating sliding

Dhieb, H.; Tabatabaei, S.A.; Gordeev, G.; Buijnsters, J. G.; Celis, J.P.

DOI

[10.1016/j.compositesb.2016.12.045](https://doi.org/10.1016/j.compositesb.2016.12.045)

Publication date

2017

Document Version

Final published version

Published in

Composites Part B: Engineering

Citation (APA)

Dhieb, H., Tabatabaei, S. A., Gordeev, G., Buijnsters, J. G., & Celis, J. P. (2017). Numerical modelling and experimental validation of debonding and heat transfer of carbon fiber reinforced composite under reciprocating sliding. *Composites Part B: Engineering*, 114, 432-444. <https://doi.org/10.1016/j.compositesb.2016.12.045>

Important note

To cite this publication, please use the final published version (if applicable). Please check the document version above.

Copyright

Other than for strictly personal use, it is not permitted to download, forward or distribute the text or part of it, without the consent of the author(s) and/or copyright holder(s), unless the work is under an open content license such as Creative Commons.

Takedown policy

Please contact us and provide details if you believe this document breaches copyrights. We will remove access to the work immediately and investigate your claim.



Numerical modelling and experimental validation of debonding and heat transfer of carbon fiber reinforced composite under reciprocating sliding



H. Dhieb^{a,*}, S.A. Tabatabaei^a, G. Gordeev^b, J.G. Buijnsters^c, J.P. Celis^a

^a Department of Materials Engineering, KU Leuven, Kasteelpark Arenberg 44, B3001 Leuven, Belgium

^b Institute of Mathematics, Informatics and Physics, Udmurt State University, Universitetskaya str. 1, 426034 Izhevsk, Russia

^c Department of Precision and Microsystems Engineering, Research Group of Micro and Nano Engineering, Delft University of Technology, Mekelweg 2, 2628 CD Delft, The Netherlands

ARTICLE INFO

Article history:

Received 14 February 2016

Received in revised form

19 December 2016

Accepted 22 December 2016

Available online 27 December 2016

Keywords:

Carbon fibers

Debonding

Cohesive interface modelling

ABSTRACT

Compressive and shear stresses as well as the generation of heat are critical issues in the failure mechanism of carbon fiber reinforced epoxy composites under reciprocating sliding. In this work, the mechanical stress distribution and maximum surface temperature generated on the wear track by reciprocating sliding against stainless steel counter body are modelled numerically. The computational results are used to directly compare them to experimental data to discuss the contact status and failure mechanism during the sliding process applying different sliding frequency and external environment. The debonding between the carbon fibers and the epoxy is modelled considering a cohesive interface modelling. We demonstrate numerically that the sliding frequency has a significant effect on heat generation. Experimentally, at higher frequencies, a more pronounced debonding and crack formation take place in the sub-surface region which is not the case at lower sliding frequencies. Water acts as a cooling agent and decreases the debonding because it functions as a plasticizer agent for the epoxy matrix.

© 2016 Elsevier Ltd. All rights reserved.

1. Introduction

There is a strong increase in usage and diversity of natural materials such as nanocrystalline cellulose [1–3] as well as synthetic carbon fibers as reinforcements in composites for engineering applications. Due to the experimental limitations to fully understand their failure, interface elements are increasingly used for modelling composites, particularly in relation to delamination [4–6] and adhesive non-line failure [7–9]. They are able to model multiple crack paths without the need for computationally expensive crack path following algorithms. In addition, they do not require the direction of crack propagation to be known in advance, and cracks have the potential to propagate along any path where interface elements are placed [10].

Friction occurring from reciprocating sliding contacts is transformed into internal energy or heat, which causes the temperature

of the sliding bodies to increase. This temperature rise associated with this heating can have an important influence on the tribological behavior of the sliding components. The generated heat may vary from one speed to another, and the exact temperatures of the contact are unknown for certain. Recording the exact temperature of the contact in situ is practically not feasible for the case of reciprocating sliding especially with small displacement amplitude. Experimental work can be used to quantify how carbon fiber reinforced epoxy composites are affected by the environment, but the underlying mechanisms remain difficult to be unraveled experimentally. The ability to predict the surface temperature and the temperature distribution of actual contacting bodies is important because tribological degradation needs to be controlled or avoided. Several methods were used in tribological systems to experimentally measure the contact temperature. However, these methods are restricted for specific tests. Alternatively, simulation prediction might be the future reliable technique to estimate the temperature map of the sliding contacts. Blok [11] studied and investigated frictional heating and contact temperatures for the first time in 1937. Jaeger [12] introduced an approximate solution

* Corresponding author.

E-mail address: houcine.dhieb@mtm.kuleuven.be (H. Dhieb).

for rectangular contacts, whereas Archard [13] investigated circular contact areas. However, it is known that tribological contacts are often elliptical. Later, Kuhlmann-Wilsdorf [14] presented approximate solutions for elliptic contacts which are applicable for most of the cases. Despite all these previous solutions, accurate studies for elliptic contacts are still lacking. Several researchers [15,16] revealed that heating generated from a friction contact can cause a significant rise in the surface temperature up to the melting or softening point of the thermoplastic polymers. The temperature rise can cause a drastic change in the friction and wear behavior of the polymer. In fact, Lancaster [15] showed that the combination of contact pressure and sliding speed causes the surface temperature to reach the critical temperature of the used materials. Ettles and Shen [17] described that even if the surface temperature does not reach the critical temperature, the viscoelastic behavior of the polymer or elastomer can be significantly affected and the resulting friction can be altered. Rozeanu and Pnueli [18] reported that contact temperatures and the resulting thermal stresses can play an important role in wear of sliding components. The fact that temperature gradients around the contacts are very large can be responsible for softening and shear failure of the sub-surface of the material. Furthermore, Ting [19] stated the responsibility of the thermomechanical stress field around a sliding contact of wearing the contacting materials. Tensile strength and modulus are affected by temperature. Their changes may occur even below the glass transition temperature. Detassis et al. [20] studied the interfacial shear strength on sized and de-sized carbon fiber reinforced epoxy as a function of temperature. They recorded an interfacial shear strength decrease with temperature. Zhuang and Wightman [21] also studied the effect of temperature on interfacial shear strength in carbon fiber epoxy composites using single fiber fragmentation testing. Temperature increment to 80 °C decreases sharply the interfacial shear strengths of three different types of fibers in epoxy which coincides with the degradation of the carbon fiber/epoxy interface region. Similar results were found on unidirectional carbon fiber reinforced polyphenylene sulfide composites by Loverich et al. [22] at room temperature and 90 °C. Comparable results concerning composite strength in the work of Reifsnider and Case [23] showed a decrease with temperature. Case [24] recorded also a decrease in transverse strength and stiffness properties of notched and un-notched composites at high temperature compared with experiments performed at room temperature. In addition, Obst et al. [25] recorded a 23% decrease of interlaminar shear strength at 121 °C by short-beam four-point bend tests.

From the previous studies, it is found that friction heat generated will reduce the performance of the composite in different aspects. It can also lead to premature failure. In more detail, when a composite surface reaches a specific temperature and stress level, a crack nucleation and further propagation will lead to a debonding of the fiber reinforcements. This debonding will dramatically decrease the mechanical properties of the composite material.

In this study, cohesive elements are used to simulate the debonding and stress distribution in carbon fiber reinforced epoxy under a combination of compression and shear forces. A 3D model was implemented in the commercial finite element code ABAQUS in order to simulate crack initiation and propagation in the composite subsurface. The cohesive zone model is employed to model the interface response in epoxy matrix composites reinforced by carbon fibers. The computational results are used to directly compare them to experimental data obtained from reciprocating sliding tests.

The objective of this study is to provide a mapping of the stress distributions originated from the reciprocating sliding as well as to provide a better understanding of how generated temperature and

water can affect the debonding of the carbon fiber reinforced epoxy subsurface under the reciprocating sliding contact.

2. Experimental

The materials used in this study are bulk epoxy and carbon fiber reinforced composite. The carbon fiber reinforcements are of type STS-24K with 4000 MPa tensile strength, 240 GPa tensile modulus, 1.7% tensile elongation, 7 μm diameter and 1.75 g/cm³ density. For the production of the bulk epoxy, standard di-glycidyl ether of bisphenol A (DGEBA, Epikote 828) and Aradur 3486 (aliphatic polyamine) as hardener (ratio epikote/hardener 100/30) were used.

Reciprocating sliding tests were done using a stainless steel counter body ball with a diameter of 10 mm. Composite samples of 5 × 5 × 5 mm³ were tested under reciprocating sliding at 50% relative humidity and immersed in demineralized water, both at 23 °C, as external environment. All tests were performed for a total of 200,000 sliding cycles. A normal load of 9 N, three sliding frequencies of 1 Hz, 3 Hz, and 9 Hz, and a peak-to-peak displacement amplitude of 600 μm were used. The sliding tests were performed along a sliding axis perpendicular to but in-plane with the fiber orientation. Detailed descriptions of the experimental setup and fabrication process of the composite material are given in previous works [26,27].

3. Numerical modelling

Many models claim to be robust in their ability to adapt varying conditions and parameters, but the claims are rarely validated with experimental evidence. Where validation is offered, the model is trusted and can be used in order to decrease the number of lab experiments. Thus, the work presented in this study, both the analytical and experimental phases, provides original contributions to the literature. The cohesive model is extracted from a homogeneous model with the same dimensions as the experimental composite samples (5 × 5 × 5 mm³). The cohesive model dimensions are based on the fiber dimensions and their spacial arrangement as visualized by focused ion beam (FIB) scanning electron microscopy (SEM) cross section in order to allow for a direct comparison of the debonding locations with the experimental results. The heat model dimensions are equal to the experimental sample as well. The contact area (a) is derived from Hertz contact calculations [28].

$$a = \left(\frac{3F_n R'}{E'} \right)^{1/3} \quad (1)$$

where F_n is the normal load (N), R' is the reduced radius (m), and E' is the reduced Young's modulus (Pa).

The reduced Young's modulus is defined as:

$$\frac{1}{E'} = \frac{1}{2} \left[\frac{1 - \nu_A^2}{E_A} + \frac{1 - \nu_B^2}{E_B} \right] \quad (2)$$

where: ν_A and ν_B are the Poisson's ratios of the contacting bodies (A: ball) and (B: composite material), respectively. E_A and E_B are the Young's moduli of the contacting bodies (A: ball) and (B: composite material), respectively.

The reduced radius for the contact between two bodies is defined as:

$$\frac{1}{R'} = \frac{1}{R_A} + \frac{1}{R_B} \quad (3)$$

where:

R_A is the radius of the stainless steel ball (m).

R_B is the radius of the composite material (m). In our case, we have a flat sample so $R_B = \infty$.

3.1. Finite elements modelling

3.1.1. Debonding modelling

One of the critical issues in the application of composite materials is the interface debonding between the reinforcement part and matrix. The interface debonding is the major responsible of strength, stiffness, and fracture behavior [29,30]. It can occur under the combined action of normal stress (mode I) and shear stresses (mode II, III) at the interface. Kyo and Wing [31] reported the vital role of interfaces to the stress transfer between the fiber and matrix and interface influence on the mechanical performance and fracture behavior of composites under various loading conditions. In the present study, the concept of the “surface to surface” cohesive model [32] was used for modelling of the debonding between the carbon fiber and epoxy matrix.

Cohesive zone models are being increasingly used to simulate discrete fracture processes in a number of composite material systems. Most of these models are typically expressed as a function of traction forces caused separation. However, the debonding of epoxy matrix composites reinforced by carbon fibers caused by combined compressive and shear loads originated from reciprocating sliding movements has not been investigated.

The cohesive element/surface approach is proved to be efficient in describing brittle fracture and failure behavior in a number of cases [33–35]. It was firstly proposed by Barenblatt [36] for perfectly brittle materials. Later, Dugdale [37] extended this concept to perfectly plastic materials. Since then, the cohesive zone approach reached models of fracture of metals, ceramics, polymers, and composites. Needleman [38,39] used polynomial and then exponential types of traction-separation equations. Tvergaard [40] used a quadratic traction displacement jump form to analyze the interfaces, whereas Tvergaard and Hutchinson [41] used a trapezoidal shape in the traction-separation model to calculate the crack growth resistance of elastic-plastic solids. Xu and Needleman [42] further used the aforementioned models to study void nucleation by inclusion debonding in a crystal matrix, fast crack growth in brittle materials under dynamic loading, and dynamic crack growth at the interface of biomaterials. Camacho and Ortiz [43] employed a linear traction-separation equation with an additional fracture criterion to propagate multiple cracks along arbitrary paths during impact damage in brittle materials. Finally, Geubelle and Baylor [44] utilized a bilinear cohesive zone model to simulate the spontaneous initiation and propagation of transverse matrix cracks and delamination fronts in thin composite plates subjected to low velocity impact (see Fig. 1).

The current research aims to simulate the debonding of carbon fiber from epoxy matrix under compressive and shear loadings. The constitutive response in cohesive elements/surfaces for delamination/debonding applications is based on a traction-separation law that is characterized by peak strength N_{\max} and fracture energy (G_{TC}) as shown in Fig. 1. There are two distinguished regions for delamination/debonding modelling using the cohesive element/surface concept: damage initiation (a) and damage evolution (b).

The damage in the bulk of the material is believed to initiate when the stress or strain values reach a maximum value. In Fig. 1, N_{\max} is the maximum value of the traction reached at the interface, δ_n^{init} is the displacement jump at the start of separation or damage initiation, δ_n^{fail} denotes the completion of damage for which the

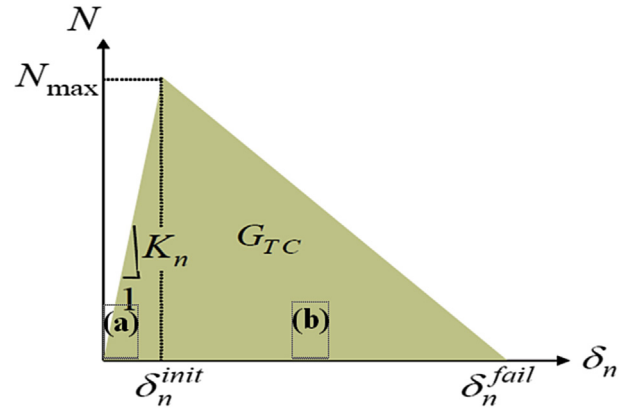


Fig. 1. Typical traction-separation response in cohesive elements/surfaces.

value of interfacial traction reduces to zero and remains zero for further increases in the value of separation. The area under the N - δ curve gives the work of separation or fracture energy denoted by G_{TC} . K_n is the elastic modulus considered as cohesive stiffness:

$$K_n = \frac{N_{\max}}{\delta_n^{init}} \quad (4)$$

In the cohesive element/surface calculations in ABAQUS, the thickness of the elements is considered as unit so the nominal strain and stress quantities are used for the traction-separation law unless the K_n values should be corrected based on the defined thickness [32].

The damage initiation criterion can be maximum nominal stress/strain criterion either in a simple form or in quadratic form that are summarized in relations (5)–(8):

- Maximum nominal stress criterion:

$$\text{MAX} \left\{ \frac{\langle \sigma_n \rangle}{N_{\max}}, \frac{\sigma_s}{S_{\max}}, \frac{\sigma_t}{T_{\max}} \right\} = 1 \quad (5)$$

- Maximum nominal strain criterion:

$$\text{MAX} \left\{ \frac{\langle \varepsilon_n \rangle}{\varepsilon_n^{\max}}, \frac{\varepsilon_s}{\varepsilon_s^{\max}}, \frac{\varepsilon_t}{\varepsilon_t^{\max}} \right\} = 1 \quad (6)$$

- Quadratic nominal stress criterion:

$$\text{MAX} \left\{ \left(\frac{\langle \sigma_n \rangle}{N_{\max}} \right)^2 + \left(\frac{\sigma_s}{S_{\max}} \right)^2 + \left(\frac{\sigma_t}{T_{\max}} \right)^2 \right\} = 1 \quad (7)$$

- Quadratic nominal strain criterion:

$$\text{MAX} \left\{ \left(\frac{\langle \varepsilon_n \rangle}{\varepsilon_n^{\max}} \right)^2 + \left(\frac{\varepsilon_s}{\varepsilon_s^{\max}} \right)^2 + \left(\frac{\varepsilon_t}{\varepsilon_t^{\max}} \right)^2 \right\} = 1 \quad (8)$$

where σ_n , σ_s , σ_t are the nominal stress in pure normal mode, first shear direction and second shear direction, respectively. S_{\max} is the maximum stress along the first transverse direction and T_{\max} is the maximum stress along the second transverse direction. Moreover, ε_n , ε_s , ε_t are the nominal strain in pure normal mode, first and second shear directions. In the finite element model of the delamination/debonding using the cohesive element/surface, the

damage evolution region is based on energy or displacement. So, the total fracture energy or the post damage-initiation effective displacement at failure should be defined. It is also possible to define a mixed mode damage condition.

The fracture energy can be defined as a function of mixed mode as following:

- Power law

$$\left(\frac{G_I}{G_{IC}}\right)^\alpha + \left(\frac{G_{II}}{G_{IIC}}\right)^\alpha + \left(\frac{G_{III}}{G_{IIIC}}\right)^\alpha = 1 \tag{9}$$

- Benzeggagh-Kenane (BK) method

$$G_{IC} + (G_{IIC} - G_{IC}) \left(\frac{G_{shear}}{G_T}\right)^\eta = G_{TC}, G_{shear} = G_{II} + G_{III}, G_T = G_I + G_{shear} \tag{10}$$

where G_I and G_{II} and G_{III} are the fracture energy release rates in the normal, first shear and second shear directions. Accordingly, G_{IC} , G_{IIC} , and G_{IIIC} are the critical fracture energies in the normal, first and second shear directions. The amount of G_{shear} in the Benzeggagh-Kenane (BK) method is a combination of fracture energies in the first and second shear directions [32]. The coefficients α and η depend on the degradation profile in the damage evolution region that can be any curve such as linear or exponential. Finally, the post damage-initiation effective displacement is calculated as following:

$$\delta = \sqrt{\delta_n^2 + \delta_s^2 + \delta_t^2} \tag{11}$$

The stiffness properties of the carbon fibers and cohesive properties at the interface that are used in the present study are summarized in Tables 1 and 2, respectively. In this model, the cohesive properties were carefully taken from other researches [45–47] that dealt with the same matrix/reinforcement and highly comparable mechanical properties, because these values are not easily measured experimentally. Fracture energies can be measured, or obtained and evaluated using standard tests as was reported by Maimi et al. [48].

The homogenized stiffness properties of the fabric are calculated using Chamis [49] formulae using constituent mechanical properties of carbon fiber and epoxy matrix for the total fiber volume fraction of 67% ($VF = 67\%$). It is similar to the “rule of mixtures” in order to obtain the stiffness properties of a composite material using the mechanical properties of its constituents: fiber and matrix. The Young’s modulus and the Poisson’s ratio of the epoxy matrix are equal to 3 GPa and 0.35, respectively.

K_{nn} , K_{ss} , and K_{tt} are the cohesive stiffnesses in the normal, first and second transverse directions. In addition, δ_n , δ_{t1} and δ_{t2} are the maximum separation displacements along the normal, and transverse directions. G_{1c} is the fracture energy at the carbon-epoxy interface. To model the debonding of single carbon fibers from the epoxy matrix on the micro-scale, it is needed to calculate the transferred forces/stresses at the surface of the sample during the reciprocating sliding on the macro-level. The reciprocating sliding condition is separated into compressive and shear forces/stresses

based on a geometrical model of the sliding ball and mechanical properties of the matrix that is in contact with the ball. The contact stresses are calculated using Hertz’s contact formulae [50].

The maximum and average contact pressures are calculated following:

$$P_{max} = \frac{3F_n}{2\pi a^2} \tag{12}$$

$$P_{average} = \frac{F_n}{\pi a^2} \tag{13}$$

The maximum shear stress is calculated from:

$$\tau_{max} = \frac{1}{3}P_{max} \tag{14}$$

The reciprocating sliding of the contact ball at the macro-level causes the debonding between the fiber and matrix at the micro-level. Therefore, a multiscale approach was implemented to find the compressive and shear components of Hertz’s stress at the micro-level. Here, for the sake of simplicity, the transferred displacements from the macro-level into the micro-unit cell were used in numerical simulations. Then, the compressive and shear stresses were applied to the upper surface of the macro-unit cell (Fig. 2b). Moreover, the two surfaces are considered smooth and no roughness is introduced, assuming that the asperity peaks from the roughness will be elastically deformed by the applied normal load and the contact area will be relatively similar. The homogenized stiffness properties of the carbon fibers are shown in Table 1.

The ball contacts with the composite materials along the sliding line with the length of 600 μm . A micro-unit cell with the dimensions of $25 \times 25 \times 5 \mu\text{m}^3$ was considered beneath the contact line. In this way, the macro-displacements during the sliding can be read at the edges of the micro-unit cell. Then, the derived displacements were applied to the micro-unit cell. In addition, the cohesive contact properties shown in Table 2 were used between the fiber and matrix in debonding simulation.

Having defined the displacements at the micro-level, the “surface to surface” cohesive interaction is defined between the fibers and matrix. Then, the stress distribution and contact status are calculated. It is noticed that the fibers location could influence the modelling results. Thus, the carbon fiber distribution in the model is drawn based on a cross-section of a tested sample (Fig. 3).

3.1.2. Finite element modelling results of debonding

The cohesive zone approach is chosen for our numerical study. A multiscale modelling approach is adopted here to predict the stress and the localized debonding. Following, experimental tests will be performed to validate the numerical results. The cohesive model will help to understand the damage initiation and crack propagation as well as the role of the interface between the matrix and fibers in the overall mechanical response of the composite. The stress distribution in the fibers and matrix during one cycle of reciprocating sliding is shown in Fig. 4. Fig. 4a and b shows the stress distribution in the matrix and carbon fibers during the first sliding action, respectively. Fig. 4c and d represent the same results but during the second (opposite) sliding movement. The stress components are compressive stress of 100 MPa along the y

Table 1
Stiffness properties of the carbon fibers.

E_{11} (GPa)	E_{22} (GPa)	E_{33} (GPa)	ν_{12}	ν_{13}	ν_{23}	G_{12} (GPa)	G_{13} (GPa)	G_{23} (GPa)
230	15	15	0.2	0.2	0.35	22	22	5.55

Table 2
Cohesive properties at the interface of carbon fiber and epoxy matrix.

K_{nn} (N/ μm^3)	K_{ss} (N/ μm^3)	K_{tt} (N/ μm^3)	δ_n (μm)	δ_{t1} (μm)	δ_{t2} (μm)	G_{1c} (N/ μm)
0.0001	0.0001	0.0001	0.02	0.02	0.02	0.00026

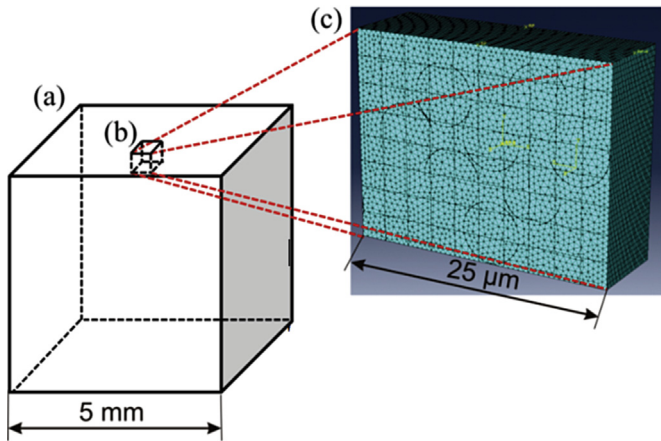


Fig. 2. The multi-scale model for calculation of boundary conditions in the micro-unit cell: a) macro-model, b) micro-model partitioned from the macro-model, and c) micro-unit cell with unidirectional carbon fibers and epoxy matrix.

direction and shear stress of 35 MPa in the x direction in the global coordinate system (GCS). The modelling shows that the Von Mises stresses (MPa) are anisotropically distributed in the micro-unit cell and are highest in the regions where the distance between fibers is minimal and the epoxy matrix extent is limited. It is shown that the elastic stress field is amplified in regions near carbon fiber/epoxy interfaces. Sliding in onward and backward directions results in similar absolute values of the Von Mises stresses, i.e. about 517 MPa in the epoxy matrix and 1,135 MPa in the fibers. ABAQUS extrapolates the integration point values to the nodes then averages the values. Avg. 75% thus implies that 75% of the values at the elements/nodes are averaged and displayed.

The contact status around the carbon fibers and the epoxy matrix in both reciprocating sliding directions is shown in Fig. 5. The contact conditions can be categorized as sticking, slipping, and opening. In the forward direction (Fig. 5a and b), the debonding (opening) of fibers 1 to 7 from the matrix occurs around the right and left edges, whereas for fibers 8 and 9 it is on the top and bottom

edges. On the other hand, for the opposite sliding direction (Fig. 5c and d), the debonding of the fibers takes place at different locations mainly on the side edges.

It is noticed that the sticking contact conditions of fiber/matrix are located at locations of highest stresses due to the compression of the matrix in y direction. On the other hand, the opening of fiber/matrix is encountered at locations of high tensile stresses of the matrix in x direction.

3.2. Heat modelling

The potential effects of generated heat due to reciprocating sliding are as important as the normal and shear effects. Just as other environmental parameters, for carbon fiber reinforced epoxy composites, changes in response with temperature are dependent on changes in matrix and interfacial regions. Carbon fibers tend to be unaffected up to temperatures of 600 °C [28]. Little work is reported in the literature regarding debonding and degradation at elevated temperature. Generated temperature from the reciprocating stainless steel counter body will be simulated and the effect of sliding frequency and heat convection will be discussed.

In this study, the finite element method is used to investigate the effect of thermal loading on the generated temperature field within the composite material. The 3D temperature distribution is modelled for the sliding system (cubic composite sample/stainless steel ball) with frictional heating due to the reciprocating sliding movement, with and without immersion in water.

The specific situation addressed in this paper, is that of a moving heat source originated from the stainless steel counter body movement on a stationary composite material. In this case, there is a relative sliding between the source of heat and the composite into which the heat flows. A model will be used to predict the maximum surface temperature on the carbon fiber reinforced epoxy composite and experimental results will be discussed to distinguish a correlation between the contact temperature and the degradation of the samples. The dimensions of the model are the same as the actual composite test samples, i.e. the size of the cubic side edge is equal to 5 mm. The heat model parameters are listed in Table 3 [51–53]. A tetrahedral mathematical mesh is used with a finer

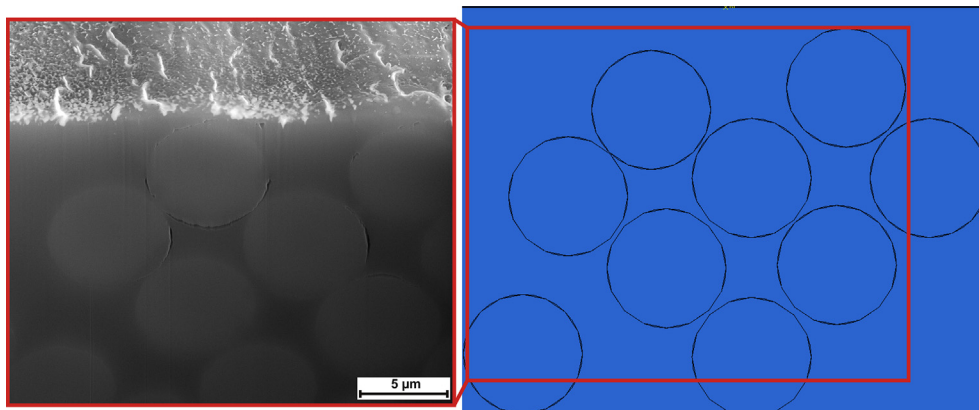


Fig. 3. One unit cell illustration: a) FIB cross-section after 300 reciprocating sliding cycles and b) unit cell from ABAQUS.

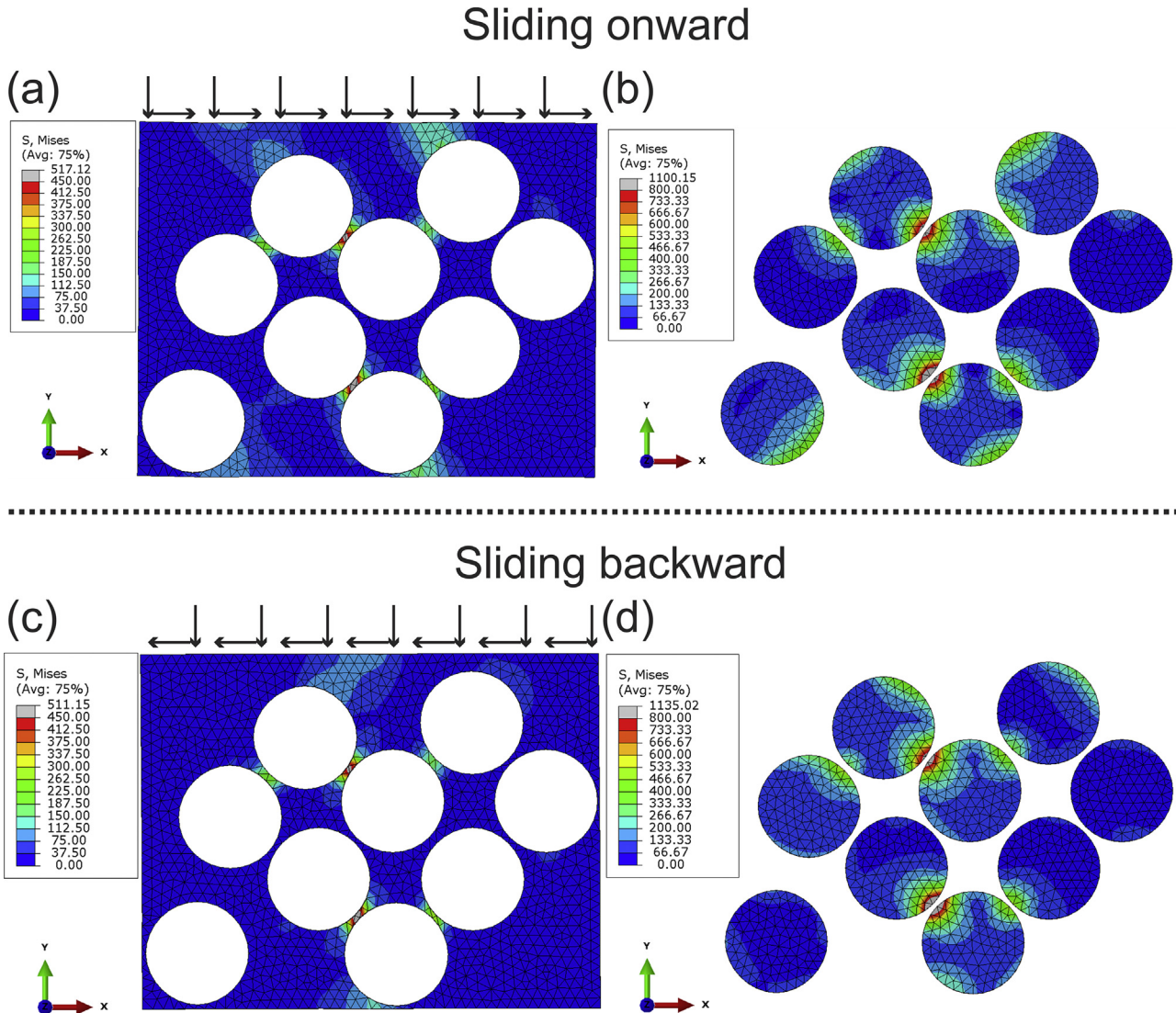


Fig. 4. Modelled stress distribution in the micro-unit cell during one reciprocating sliding cycle: (a) and (c) matrix, (b) and (d) fibers. Images (a) and (b) present the modelling results of the forward motion, whereas (c) and (d) show those of the backward motion (indicated by the black arrows in the x direction).

mesh size in the contact area $\partial\Omega_{\text{FRICTION}}$ (see Fig. 6). Two bodies are used for the reciprocating sliding tests in which the first body is the carbon fiber reinforced epoxy sliding with fixed relative distance equal to 600 μm and with different frequencies. The second body is the stainless steel ball counter body with 10 mm diameter. It is assumed that all the energy is dissipated as heat on the sliding surface of the carbon fiber reinforced composite and is conducted into the composite with no heat loss. The accuracy of a model that attempts to incorporate different frequencies and environments only by changing the speed or the heat convection values allows for an approximate estimation of the temperature rise.

The sliding conditions examined for the heat simulation are: in ambient air (23 °C, 50% RH) at 1 Hz (1) and 3 Hz (2), immersed in water (23 °C) at 3 Hz (3), in ambient air at 5 Hz (4) and 9 Hz (5), and immersed in water at 9 Hz (6).

The reciprocating sliding of the stainless steel ball against the carbon fiber reinforced epoxy occurs in a relatively small contact area. The carbon fiber reinforced epoxy is an anisotropic material. However, to simplify the calculation the thermal conductivity k is chosen as scalar by assuming isotropic thermal properties of the composite material. The external environment is taken into

consideration by changing the heat transfer coefficient for either ambient air or water immersion.

The partial differential equation is expressed as following:

$$\rho C_p \frac{\partial T}{\partial t} - \nabla \cdot (k \nabla T) \Big|_{\Omega} = 0 \quad (15)$$

where T is the temperature of the composite material, t is the time, ρ is the density of the composite material, k is the thermal conductivity and C_p is the heat capacity of the composite material.

The following boundary conditions apply:

$$-\mathbf{n} \cdot (-k \nabla T) \Big|_{\partial\Omega_{\text{FRICTION}}} = F + h_{ts}(T_{\text{amb}} - T) \quad (16)$$

$$-\mathbf{n} \cdot (-k \nabla T) \Big|_{\partial\Omega} = h_{ts}(T_{\text{amb}} - T) \quad (17)$$

$$T \Big|_{\partial\Omega_{\text{BOTTOM}}} = T_{\text{amb}} \quad (18)$$

where $\partial\Omega_{\text{FRICTION}}$ (Fig. 6a) is the boundary of the area where the counter body slides against the composite material. $\partial\Omega$ (Fig. 6a) is the rest of the edge boundaries. $\partial\Omega_{\text{BOTTOM}}$ is the bottom boundary of

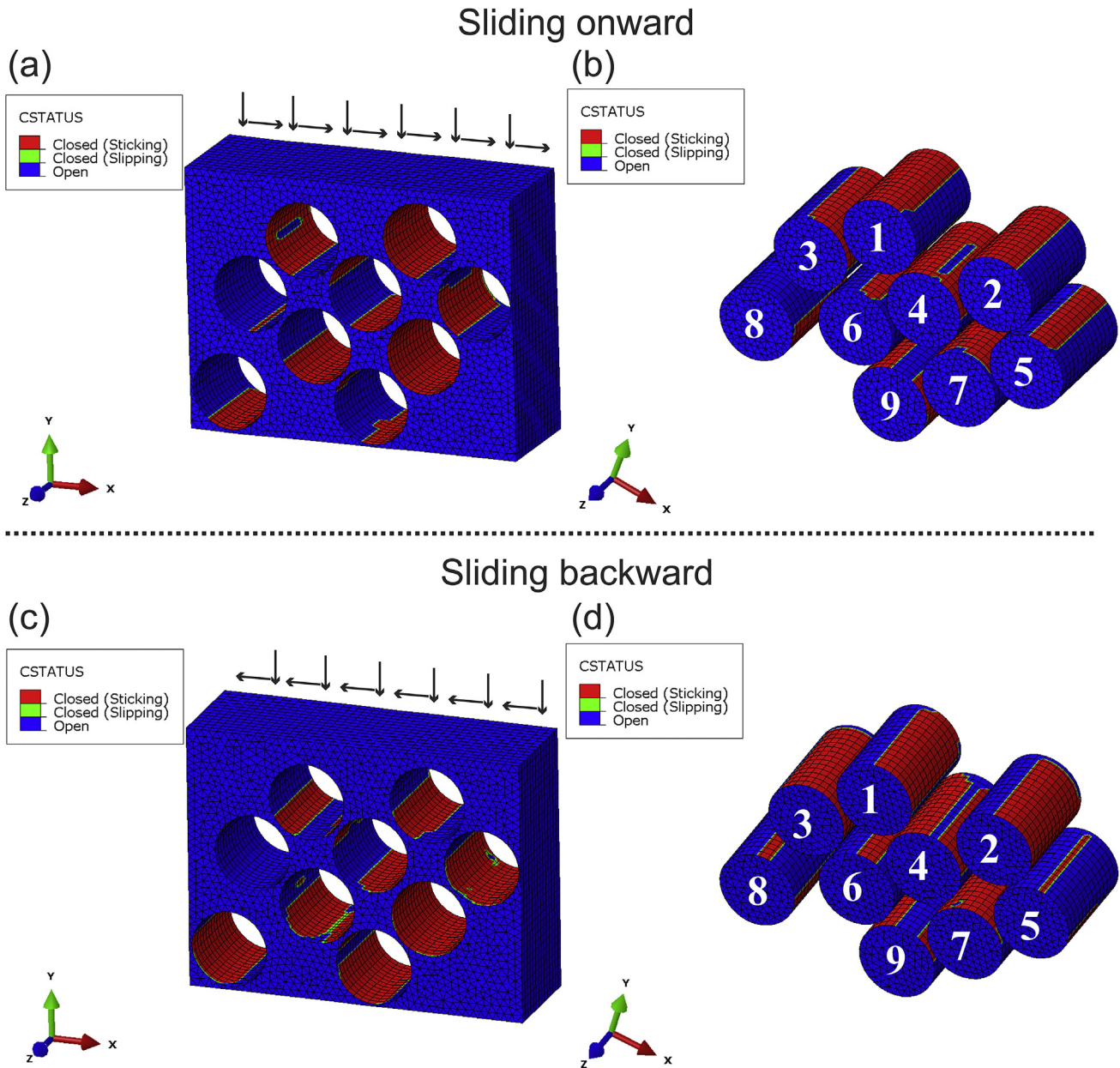


Fig. 5. Modelled contact conditions (i.e., sticking, slipping and opening) in one reciprocating sliding cycle: (a) and (c) around the matrix surfaces, (b) and (d) around the fiber surfaces.

Table 3
Heat model parameters.

Symbol	Value	Description
ρ	1600 [kg/m ³]	Density of the composite material [47]
C_p	950 [J/(kg K)]	Heat capacity of the composite material [47]
k	0.25 [W/(m K)]	Thermal conductivity of the composite material [47]
h_{air}	10 [W/(m ² K)]	Heat transfer coefficient for air [48]
h_{wat}	80 [W/(m ² K)]	Heat transfer coefficient for water [49]
T_{amb}	23 °C	Temperature of the ambient
Q_c	0.005 [J]	Amount of energy dissipated during one friction cycle
t_c	6 [min]	Time of the running model
$S_{FRICTION}$	$6.6 \cdot 10^{-7}$ [m ²]	Area of the boundary $\partial\Omega_{FRICTION}$

the composite material. The normal vector \mathbf{n} is directed from the ambient into the composite material. $h_{ts}(T_{amb} - T)$ is responsible for convection cooling, where h_{ts} is the heat transfer coefficient;

$h_{ts} = h_{air}$ if the environment is ambient air and $h_{ts} = h_{wat}$ if the composite is immersed in water. T_{amb} is the ambient temperature. F is the thermal source and is expressed as:

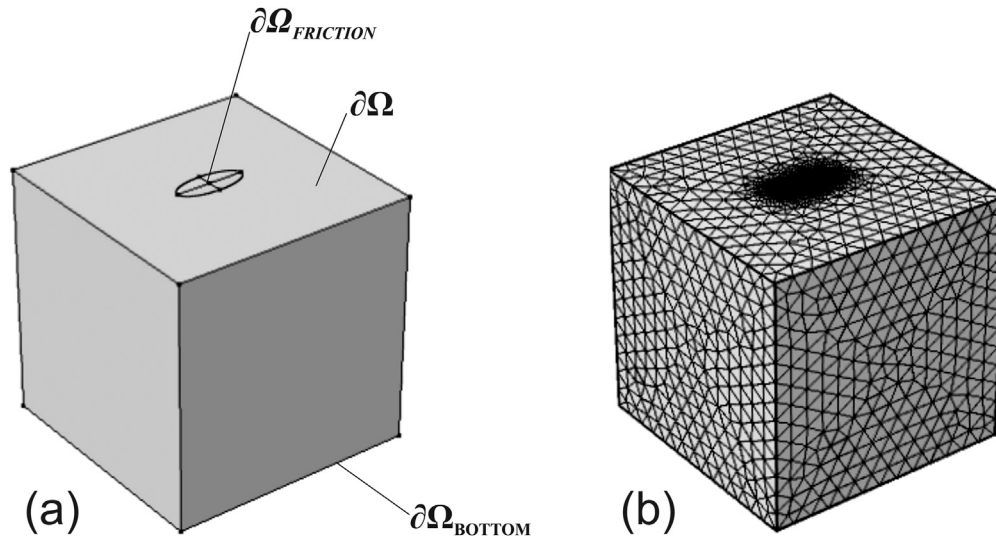


Fig. 6. The heat model: (a) contact zone/edges and (b) meshed model.

$$F = \frac{Q_c}{t_c S_{\text{FRICTION}}} \quad (19)$$

where t_c is the time of one reciprocating sliding cycle, S_{FRICTION} is the contact area and Q_c is the dissipated energy for one reciprocating cycle. Q_c can be expressed as:

$$Q_c = \int F_t \cdot dx \quad (20)$$

where F_t is the immediate tangential force recorded during sliding. The average coefficient of friction μ is then given by:

$$\mu = \frac{Q_c}{2 \cdot F_n \cdot d} \quad (21)$$

where F_n is the normal load and d is the reciprocating displacement.

The initial condition of the model is:

$$T = T_{\text{amb}} \quad (22)$$

The equations given above are solved via the finite element method in the classical formulation of the Galerkin method in COMSOL Multiphysics [54].

It is found that a steady-state condition is already reached after the first few seconds. The steady-state temperature is plotted through the entire material thickness for each of the six different sliding conditions (Fig. 7). It is clear that the temperature decreases from the sliding surface to the sample bottom. The generated heat that enters the composite is concentrated in the top surface under the reciprocating sliding contact. Due to the repeatable sliding movement, the heat source passes repeatedly over the same area on the wear track. There unavoidably exists an extra surface temperature rise because the frictional heat generated during one pass cannot completely flow away from the contact area before the next generation of heat at the same spot. Fig. 7 shows that the maximum surface temperature is located at the surface contact (i.e., at zero depth distance) and it decreases throughout the depth of the sample till it reaches the ambient temperature located at the bottom edge (23 °C). The sliding frequency is the origin of the temperature difference between the different tests, i.e. the higher the frequency the higher the generated temperature is. The maximum

steady-state temperature of about 140 °C is obtained for reciprocating sliding at 9 Hz in ambient air. By immersing the composite in water, the maximum surface temperature at 9 Hz drops to about 60 °C. Note that the temperature profiles simulated for sliding at 1 Hz in ambient air of 50% RH and at 3 Hz with water immersion are practically overlapping. The same is true for sliding at 3 Hz in ambient air and at 9 Hz in water. This shows the very effective cooling of the composite material by the water surrounding it.

It is concluded from the model that a steady state condition is reached in a very short time for each condition after reciprocating sliding commences, so nearly all the time of reciprocating sliding is spent in steady state conditions. Jaeger [12] found similar results for sliding or cutting contacts. Bhushan [55] analyzed the time needed for the temperature to reach the steady state value and found that the flash temperature is reached after moving a distance of only 1.25 times the length of the heat source. It is also noticed that the heat distribution is located mostly in the top 0.5 mm before 50% gradual decrease in the temperature from the maximum surface temperature.

4. Experimental results

Experimental reciprocating sliding tests were done using the same conditions as those selected for the heat modelling to allow for a direct comparison between the heat and debonding models and experimental observations.

Surface and sub-surface degradation of the epoxy composite after 200,000 reciprocating sliding cycles against stainless steel ball with 3 Hz in ambient air is displayed in Fig. 8. The sliding direction is indicated by arrows, and the carbon fiber orientation is specified by 4 parallel lines. The cross section through the wear track shows cracks and extended debonding along the interface between the epoxy matrix and the carbon fibers located in the first layer (Fig. 8b). The wear track surface tested in ambient air with 3 Hz shows clearly the carbon fibers and the matrix. In the second experiment, demineralized water was added to the sliding system thereby maintaining the same frequency but changing the environment in order to decrease the heat generation. Top-view SEM and FIB-SEM cross section images are shown in Fig. 9. On the one hand, a significant increase of the wear track size is recorded (around 3 times bigger). On the other hand, a significant reduction of the debonding of the interface is noticed.

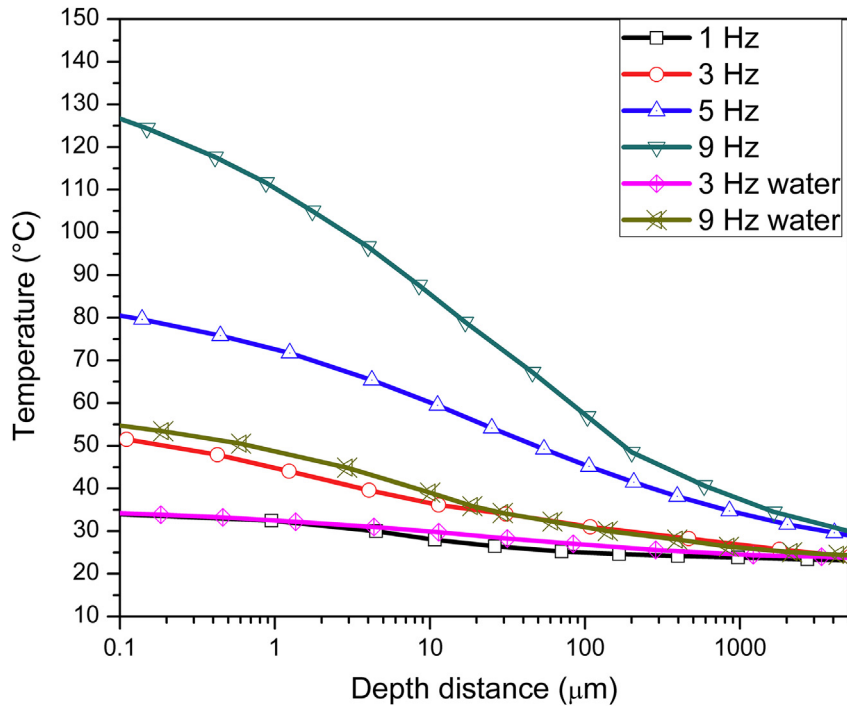


Fig. 7. Finite element calculation of the steady-state temperature at the center of the sliding contact towards the composite bottom as a function of the depth distance with different sliding frequencies for reciprocating sliding at 50% RH or immersed in water.

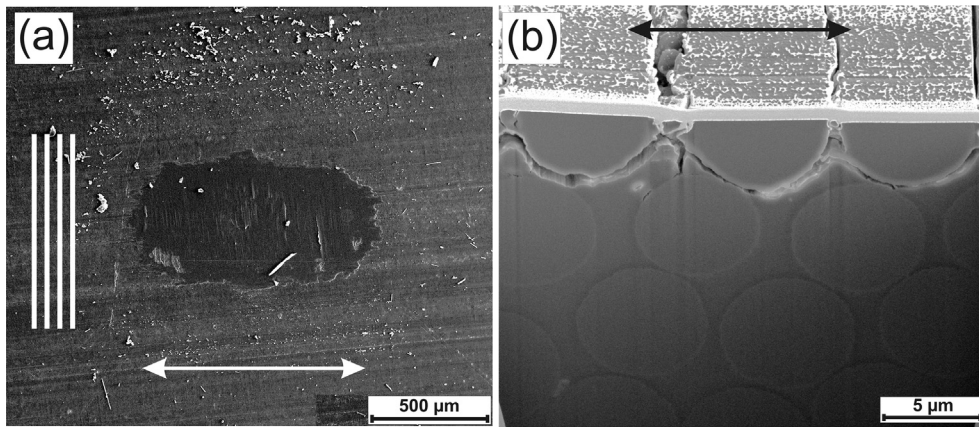


Fig. 8. (a) Top-view SEM image and (b) FIB-SEM cross section of the wear track on carbon fiber reinforced epoxy after 200,000 reciprocating cycles performed against stainless steel in ambient air with 3 Hz frequency.

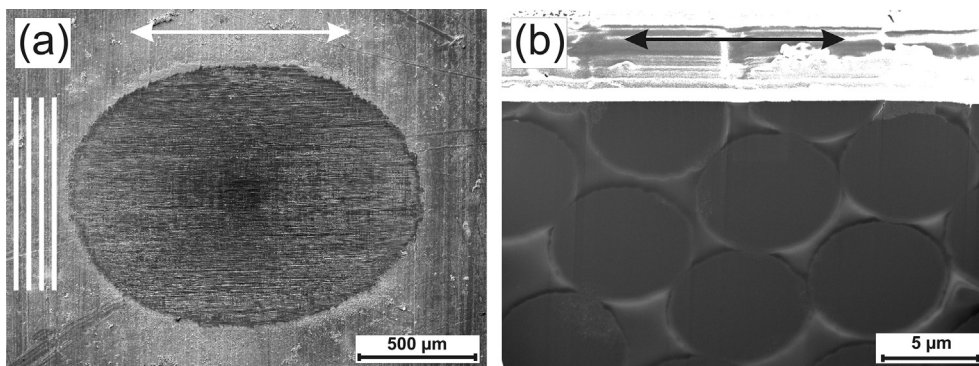


Fig. 9. (a) Top-view SEM image and (b) FIB-SEM cross section of the wear track on carbon fiber reinforced epoxy after 200,000 reciprocating cycles performed against stainless steel in demineralized water with 3 Hz frequency.

At ambient air with 1 Hz (Fig. 10), the wear track area is slightly smaller than with 3 Hz (Fig. 8), and the cross section shows a very limited debonding and the surface remains covered by epoxy matrix. The consumption of the top surface is remarkably lower as evidenced by the remaining epoxy layer and the decrease of the wear track size.

Reciprocating sliding with a frequency of 9 Hz is tested in ambient air and in demineralized water. A clear wearing off of the top surface is noticed combined with a strong debonding of the top layer of carbon fibers in ambient air (Fig. 11). Tests done in demineralized water again show an increase of the wear track size (Fig. 12a). This increase is the result of the higher wear of the composite material.

Water plays three roles: a cooling agent which decreases the surface temperature from 140 °C at 9 Hz to 35 °C at 1 Hz, a plasticizer which holds the stresses and decreases the debonding between the carbon fibers and the matrix, and a wearing accelerator which increases the consumption of the top layer of the composite material.

Based on the modelling and the experimental results, surface and sub-surface temperatures can become high enough to cause changes in the structure and properties of the sliding materials, oxidation of the surface, and possibly even melting of the contacting solids. In our study, the pressure was maintained constant and the frequency was changed to vary the maximum surface temperature. In the experiments performed at 3 Hz and 9 Hz (in 50% RH) where there is a relatively high generated temperature, a significant debonding is taking place in the interface between the carbon fibers and the epoxy matrix (Figs. 8 and 11). This phenomenon is less noticeable or absent in low generated temperature by either low sliding frequency or by adding water in the system (Figs. 9, 10 and 12).

5. Discussion

Our debonding model proves that carbon fiber reinforced epoxy composite is extremely susceptible to crack initiation and growth preferentially along the interfaces. Debonding and crack growth are the most prevalent life-limiting for unidirectional carbon fiber reinforced epoxy composites. When subjected to reciprocating sliding, complex loads are applied namely normal load and shear forces which can lead to critical failure of the composite sample. The Von Mises stresses between the epoxy and carbon fibers vary from around 520 MPa–1100 MPa respectively and lead the debonding to occur. The high stresses are located in the area where

there is a limited amount of epoxy between two carbon fibers. In other words, the epoxy leads the stresses to dissipate throughout the bulk due to its high elastic and plastic deformations comparing with the carbon fiber reinforcements. The stresses in cyclic reciprocating sliding can cause fatigue and more pronounced debonding by the repeatability of sticking-opening phenomena. The discontinuity of the load capacity gives rise to interlaminar stresses. In addition to the mechanical loading, delamination may result from large differences in temperature and external environment [4]. In general, degradation will be subjected to a crack driving force with a mode I opening, a mode II forward shear. Therefore, delamination in typical composites is always a mixed mode fracture process.

Our heat modelling predicts the generated heat from the sliding motions in different environments. When these results are correlated with the experimental results, it is found that temperature may play a major role on the degradation/debonding of the composite. Applying a sliding frequency of 1 Hz does not allow the surface to reach a critical temperature (35 °C) which leads the composite to debond (Fig. 7). In other words, the interaction time of the contact zone with the outside environment is long enough to maintain the temperature relatively close to the ambient temperature (23 °C). The high contact temperatures and large temperature gradients generated at higher frequencies (e.g., 9 Hz) can reach 140 °C (Fig. 7) and can be responsible for large thermomechanical stresses which cause thermocracking of the sliding surfaces. This temperature is higher than the measured glass temperature (T_g) of the composite samples (120 °C) [27] which explains the significant surface and sub-surface degradation. The maximum surface temperature estimated from the model at 3 Hz sliding frequency is about 60 °C. The tests done in full water immersion could not reach higher temperature than the T_g as a result of convective heat transfer of the water. Lancaster [15] showed that the PV limit which is often used in the design of dry plastic bearings, is in reality a critical surface temperature limit. In other words, the combination of contact pressure and sliding velocity causes the surface temperature to reach the critical temperature of the material. Ettles and Shen [56] revealed that even if the surface temperature does not reach the critical temperature, the viscoelastic behavior of the elastomer can be significantly affected and the resulting friction can be altered.

When the ball counter body slides against the composite material, friction will occur. Mechanical energy is transformed into internal energy and heat, which causes the temperature of the sliding bodies to increase. In all available literature, the exact mechanism by which this energy transformation occurs, the

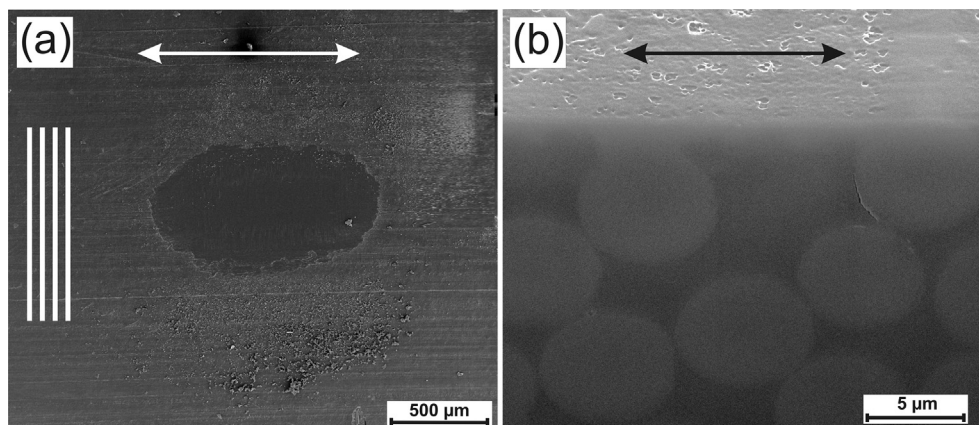


Fig. 10. (a) Top-view SEM image and (b) FIB-SEM cross section of the wear track on carbon fiber reinforced epoxy after 200,000 reciprocating cycles performed against stainless steel in ambient air with 1 Hz frequency.

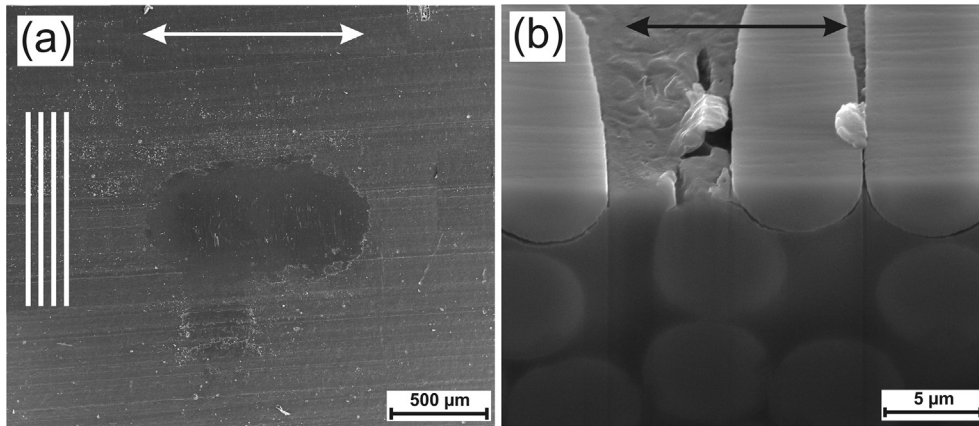


Fig. 11. (a) Top-view SEM image and (b) FIB-SEM cross section of the wear track on carbon fiber reinforced epoxy after 200,000 reciprocating cycles performed against stainless steel in ambient air with 9 Hz frequency.

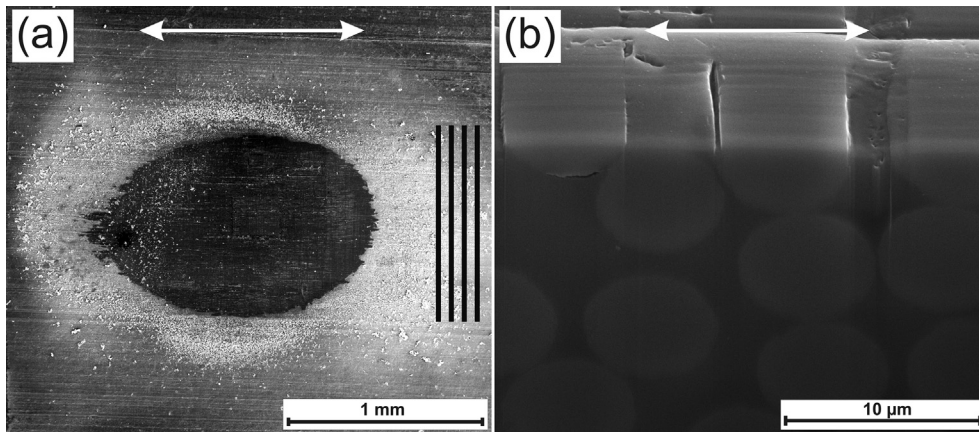


Fig. 12. a) Top-view SEM image and (b) FIB-SEM cross section of the wear track on carbon fiber reinforced epoxy after 200,000 reciprocating cycles performed against stainless steel in demineralized water with 9 Hz frequency.

partition and the temperature values are not given with great accuracy. It is known that heat originated from sliding movement is concentrated within limited special areas of contact between the two bodies in motion. Uetz and Föhl [57] showed that most of the dissipated energy generated from frictional contacts is transformed into heat. Rigney and Hirth [58] believe that most dissipated energy occurs in the solid beneath the contact region by plastic deformation processes. Kennedy [59] has shown experimentally that at least 95% of the dissipated energy occurs within the top 5 μm of the contacting bodies. Landman et al. [60] contend that these processes occur by atomic scale interactions within the top several atomic layers on the contacting surfaces. The reciprocating sliding frequency is responsible for increases in the temperature of the ball counter body and the composite material especially within the contact region on their sliding surfaces where the temperatures are highest.

6. Conclusions

Conventional fiber reinforced polymeric composites suffer from compression, shear, and heat making them highly susceptible to crack initiation and crack growth along the interface between the carbon fibers and the epoxy matrix. By studying the numerical results, we have shown that the cohesive model and the heat

modelling are effective tools in understanding and explaining the debonding and sample degradation in different conditions of reciprocating sliding against stainless steel. A 3D cohesive model was developed to simulate a combination of compressive and shear forces on unidirectional carbon fiber reinforced epoxy. The model reveals the sticking, sliding, and opening of regions in the interfaces between the fibers and the matrix. The mapped stress is concentrated in the region where the distance between two fibers is minimal and can reach around 550 MPa in the matrix and 1100 MPa in the carbon fibers. A 3D heat model was also employed to predict the heat distribution due to the sliding movement. With the experimental results, it is proved that the sliding frequency has a great influence on the temperature variation at the sliding contact and within the composite. 9 Hz frequency generates a maximum surface temperature of around 140 °C whereas a 1 Hz frequency results in a maximum temperature of only 35 °C. Our modelling and test results show that frictional heat increases the debonding of the composite. On the other hand, immersion in water effectively cools down the surface contact to around 35 °C but it increases the surface wear by plasticization. Negligible debonding is recorded in low generated temperatures either by low frequency or by water immersion.

The numerical simulation of stress and heat distributions is a powerful tool for the modelling and understanding of the initiation

and progress of composite debonding and sub-surface degradation of fiber reinforced epoxy composite materials. Further developments are needed in order to have a dynamic simulation of composite debonding with the introduction of heat calculations.

Acknowledgements

The authors thank Prof. Stepan Lomov from KU Leuven for his fruitful discussions and valuable advices. The authors would like to thank also Dr. Katleen Vallons from KU Leuven for providing the specimens. Part of this research was done within the EU FP7-PEOPLE-2011-IRSES “Oil & Sugar”-Project (Grant Agreement No. 295202) and European's Community Seventh Framework Programme (FP7/2007-2013, theme NMP.2012.1.4–3) under grant agreement 310344. The research of one of the authors (G. G) was financially supported by RFBR (project No. 16-38-00839 mol_a).

References

- [1] Chen Y, Xu C, Huang J, Wu D, Lv Q. Rheological properties of nanocrystalline cellulose suspensions. *Carbohydr Polym* 2017;157:303–10.
- [2] Coccia V, Cotana F, Cavalaglio G, Gelosia M, Petrozzi A. Cellulose nanocrystals obtained from cynara cardunculus and their application in the paper industry. *Sustainability* 2014;6(8):5252.
- [3] Puglia D, Biagiotti J, Kenny JM. A review on natural fibre-based composites-Part II. Application of natural reinforcements in composite materials for automotive industry. *J Nat Fibers* 2005;1(3):23–65.
- [4] Wen-Guang J, Hallett SR, Breen BG, Wisnom MR. A concise interface constitutive law for analysis of delamination and splitting in composite materials and its application to scaled notched tensile specimens. *Int J Numer Methods Eng* 2007;69(9):1982–95.
- [5] Su ZC, Tay TE, Ridha M, Chen BY. Progressive damage modeling of open-hole composite laminates under compression. *Compos Struct* 2015;122(0):507–17.
- [6] Zhang C, Li N, Wang W, Binienda WK, Fang H. Progressive damage simulation of triaxially braided composite using a 3D meso-scale finite element model. *Compos Struct* 2015;125(0):104–16.
- [7] Blackman BRK, Hadavinia H, Kinloch AJ, Williams JG. The use of a cohesive zone model to study the fracture of fibre composites and adhesively-bonded joints. *Int J Fract* 2003;119(1):25–46.
- [8] Thouless MD, Li S, Waas AM, Schroeder JA, Zavattieri PD. Mixed-mode cohesive-zone models for fracture of an adhesively bonded polymer-matrix composite. *Eng Fract Mech* 2006;73(1):64–78.
- [9] Campilho RDSG, da Silva LFM. 4-Mode I fatigue and fracture behaviour of adhesively-bonded carbon fibre-reinforced polymer (CFRP) composite joints. In: Vassilopoulos AP, editor. *Fatigue and fracture of adhesively-bonded composite joints*. Woodhead Publishing; 2015. p. 93–120.
- [10] Petrossian Z, Wisnom MR. Prediction of delamination initiation and growth from discontinuous plies using interface elements. *Compos Part A-Applied Sci Manuf* 1998;29(5–6):503–15.
- [11] Blok H. Theoretical study of temperature rise at surface of actual contact under oiliness lubricating conditions. *Proc general Discuss Lubr Lubr* 1937;2:222–35.
- [12] Jaeger JC. Moving courses of heat and temperature of sliding contacts. *Proc R Soc N. S. W* 1942;76:203–24.
- [13] Archard JF. The temperature of rubbing surfaces. *Wear* 1959;2(6):438–55.
- [14] Kuhlmann-Wilsdorf D. Sample calculations of flash temperatures at a silver-graphite electric contact sliding on copper. *Wear* 1986;107(1):71–90.
- [15] Lancaster JK. Estimation of the limiting PV relationships for thermoplastic bearing materials. *Tribology* 1971;4(2):82–6.
- [16] Dowson D, Dalmaz G, Childs THC, Taylor CM. *Dissipative processes in tribology*. Elsevier Science; 1994.
- [17] Ettles CMM, Shen JH. The influence of frictional heating on the sliding friction of elastomers and polymers. *Rubber Chem Technol* 1988;61(1):119–36.
- [18] Rozeanu L, Pnueli D. Two temperature gradients model for friction failure. *Trans ASME J Lubr Technol* 1978;100(4):479–85.
- [19] Ting BY. A thermomechanical wear theory [Ph.D. dissertation]. Atlanta, GA: Georgia Institute of Technology; 1988.
- [20] Detassis M, Pegoretti A, Migliaresi C. Effect of temperature and strain rate on interfacial shear stress transfer in carbon/epoxy model composites. *Compos Sci Technol* 1995;53(1):39–46.
- [21] Zhuang H, Wightman JP. The influence of surface properties on carbon fiber/epoxy matrix interfacial adhesion. *J Adhesion* 1997;62(1–4):213–45.
- [22] Loverich JS, Russell BE, Case SW, Rifsnyder KL. Life prediction of PPS composites subjected to cyclic loading at elevated temperatures. Time dependent and nonlinear effects in polymers and composites. *ASTM STP 1357*. Philadelphia: ASTM; 2000. p. 310–7.
- [23] Reifsnider KL, Case SW. Mechanics of temperature-driven long-term environmental degradation of polymer-based composite systems vols. 69-1. ASME Materials Division American Society of Mechanical Engineers, MD; 1995. p. 225–30.
- [24] Case SW. Mechanics of fiber-controlled behavior in polymeric composite materials [Ph.D. dissertation]. Virginia Polytechnic Institute and State University; 1996.
- [25] Obst AW, VanLandingham, M. R., Eduljee, R. F., Gillespie, J. W., Griesheim, G. E., and Tosi, K. F. The effect of hughothermal cycling on the microcracking behavior of fabric laminates, In: *Technology transfer in a global community international SAMPE technical conference*. 1996;vol. 28:994–1002.
- [26] Dhieb H, Buijnsters JG, Eddoumy F, Celis JP. Surface damage of unidirectional carbon fiber reinforced epoxy composites under reciprocating sliding in ambient air. *Compos Sci Technol* 2011;71(15):1769–76.
- [27] Dhieb H, Buijnsters JG, Eddoumy F, Vázquez L, Celis JP. Surface and sub-surface degradation of unidirectional carbon fiber reinforced epoxy composites under dry and wet reciprocating sliding. *Compos Part A Appl Sci Manuf* 2013;55(0):53–62.
- [28] McLaughlin Jr PVD, McShane HA, Cochran R, Armstrong-Carroll E. Effects of high on the strength and fatigue life of unidirectional polymer-matrix composites. *Proc ASME Aerosp Mater Div* 1996;427–41. AD Vol. 51/MD Vol 73.
- [29] Jayaraman K, Reifsnider KL, Swain RE. Elastic and thermal effects in the interphase: part II. Comments Model Stud J Compos Technol Res 1993;15(1):14–22.
- [30] Dhieb H, Buijnsters JG, Elleuch K, Celis JP. Effect of relative humidity and full immersion in water on friction, wear and debonding of unidirectional carbon fiber reinforced epoxy under reciprocating sliding. *Compos Part B Eng* 2016;88:240–52.
- [31] Jang-Kyo K, Yiu-Wing M. High strength, high fracture toughness fibre composites with interface control-a review. *Compos Sci Technol* 1991;41(4):333–78.
- [32] <http://abaqus.ethz.ch:2080/v6.11/books/usb/default.htm>.
- [33] Evangelista Jr F, Roesler JR, Proença SP. Three-dimensional cohesive zone model for fracture of cementitious materials based on the thermodynamics of irreversible processes. *Eng Fract Mech* 2013;97(0):261–80.
- [34] Chakraborty P, Biner SB. A unified cohesive zone approach to model the ductile to brittle transition of fracture toughness in reactor pressure vessel steels. *Eng Fract Mech* 2014;131(0):194–209.
- [35] Yao Y, Liu L, Keer LM. Pore pressure cohesive zone modeling of hydraulic fracture in quasi-brittle rocks. *Mech Mater* 2015;83(0):17–29.
- [36] Barenblatt GI. The formation of equilibrium cracks during brittle fracture. General ideas and hypotheses. Axially-symmetric cracks. *J Appl Math Mech* 1959;23(3):622–36.
- [37] Dugdale DS. Yielding of steel sheets containing slits. *J Mech Phys Solids* 1960;8(2):100–4.
- [38] Needleman A. A continuum model for void nucleation by inclusion debonding. *Trans ASME J Appl Mech* 1987;54(3):525–31.
- [39] Needleman A. An analysis tensile decohesion along interface. *J Mech Phys Solids* 1990;38(3):289–324.
- [40] Tvergaard V. Effect fiber debonding a whisker-reinforced metal. *Mater Sci Eng A Struct Mater Prop Microstruct Process* 1990;125(2):203–13.
- [41] Tvergaard V, Hutchinson JW. The relation between crack-growth resistance and fracture process parameters in elastic plastic solids. *J Mech Phys Solids* 1992;40(6):1377–97.
- [42] Xu XP, Needleman A. Void nucleation by inclusion debonding in a crystal matrix. *Model Simul Mater Sci Eng* 1993;1(2):111–32.
- [43] Camacho GT, Ortiz M. Computational modelling of impact damage in brittle materials. *Int J Solids Struct* 1996;33(20–22):2899–938.
- [44] Geubelle PH, Baylor JS. Impact-induced delamination of composites: a 2D simulation. *Compos Part B-Engineering* 1998;29(5):589–602.
- [45] Lapczyk I, Hurtado JA. Progressive damage modeling in fiber-reinforced materials. *Compos Part A Appl Sci Manuf* 2007;38(11):2333–41.
- [46] Harper PW, Hallett SR. Cohesive zone length in numerical simulations of composite delamination. *Eng Fract Mech* 2008;75(16):4774–92.
- [47] Y. Y. Jia W, Yan, H. Y. Liu. Numerical study on carbon fibre pullout using a cohesive zone model, In: *18th International Conference On Composite Materials*; 2011.
- [48] Maimi P, Camanho PP, Mayugo J, Davilla CG. A thermodynamically consistent damage model for advanced composites. *Tech. Rep. NASA/TM-2006–214282*. 2006.
- [49] Chamis CC. Mechanics of composite materials: past, present, and future. *J Compos Technol Res* 1989;11(1):3–14.
- [50] Johnson KL. *Contact mechanics*. Cambridge University Press; 1985.
- [51] CES EduPack Granta's. Granta material intelligence. Granta Design Limited; 2007.
- [52] Jorge LMM, Jorge RMM, Fujii, Giudici R. Evaluation of heat transfer in a catalytic fixed bed reactor at high temperatures. *Braz J Chem Eng* 1999;16:407–20.
- [53] http://www.engineeringtoolbox.com/convective-heat-transfer-d_430.html.
- [54] <http://nf.nci.org.au/facilities/software/COMSOL/4.3a/doc/pdf/mph/COMSOLMultiPhysicsReferenceGuide.pdf>.
- [55] Bhusan B. Magnetic head-media interface temperatures: Part 1—Analysis. *J Tribol* 1987;109(2):243–51.
- [56] McC. Ettles CM, Shen JH. The influence of frictional heating on the sliding friction of elastomers and polymers. *Rubber Chem Technol* 1988;61(1):

- 119–36.
- [57] Uetz H, Föhl J. Wear as an energy transformation process. *Wear* 1978;49(2): 253–64.
- [58] Rigney DA, Hirth JP. Plastic deformation and sliding friction of metals. *Wear* 1979;53(2):345–70.
- [59] Kennedy FE. Single pass rub phenomena—analysis and experiment. *J Tribol* 1982;104(4):582–8.
- [60] Landman U, Luedtke WD, Burnham NA, Colton R. Atomistic mechanisms and dynamics of adhesion, nanoindentation, and fracture. *Science* 1990;248(4954):454–61.